nature neuroscience

Transfection via whole-cell recording *in vivo*: bridging single-cell physiology, genetics and connectomics

Ede A Rancz[1,2,6], Kevin M Franks[1,3,6], Martin K Schwarz[4], Bruno Pichler[2], Andreas T Schaefer[1,5] & Troy W Margrie[1,2]

Single-cell genetic manipulation is expected to substantially advance the field of systems neuroscience. However, existing gene delivery techniques do not allow researchers to electrophysiologically characterize cells and to thereby establish an experimental link between physiology and genetics for understanding neuronal function. In the mouse brain *in vivo*, we found that neurons remained intact after 'blind' whole-cell recording, that DNA vectors could be delivered through the patch-pipette during such recordings and that these vectors drove protein expression in recorded cells for at least 7 d. To illustrate the utility of this approach, we recorded visually evoked synaptic responses in primary visual cortical cells while delivering DNA plasmids that allowed retrograde, monosynaptic tracing of each neuron's presynaptic inputs. By providing a biophysical profile of a cell before its specific genetic perturbation, this combinatorial method captures the synaptic and anatomical receptive field of a neuron.

A central goal for neuroscience is to understand how neurons in the brain and spinal cord process information. Ultimately this requires information from combined electrophysiological, neuroanatomical, optical and genetic methods that together can address the necessary broad range of questions, from the level of genes and molecules up to single cells and circuits[1–9]. Electrical recording methods, such as the whole-cell patch-clamp technique, can provide a relatively complete biophysical characterization of an individual neuron. The optimization of this technique for *in vivo* applications has afforded increased stability and longevity so that the intrinsic, synaptic and spiking properties of cells in many superficial[10–13] and deep structures[14–18] have been obtained. This method has been especially useful for determining the synaptic receptive fields of single cells in anesthetized[14], awake head-fixed[14,17,19] and freely moving[20] animals so that synaptic activity can be linked directly to sensory processing[16] and behavior[17,18].

Concurrently, developments in optogenetics[8,21,22] and virus-based circuit tracing[3,4,23] have provided effective tools for manipulating and tracing neuronal circuits both *in vitro* and *in vivo*. For example, genetically controlling the expression of channelrhodopsin or halorhodopsin make it possible to selectively excite or inhibit the activity of defined sets of neurons *in vivo*[8,24]. Viral strategies for expression are also becoming increasingly useful for spatially, temporally and genetically controlling network function[3,25] and even tracing the anatomical connectivity of a single cell[26]. However, there is no method available that delivers both single-cell electrophysiology and genetic manipulation. Application of such a tool could be used to provide answers to questions that are fundamental to our understanding of the roles of single neurons in the context of a local network in an intact animal[27].

The relatively large tip size of patch pipettes not only permits low-resistance intracellular recordings but also allows researchers to dialyze exogenous materials into the recorded cell[12,14,28], which raises the possibility of delivering macromolecules such as plasmids. Here we examine the feasibility of combining *in vivo* whole-cell recording and gene delivery by answering four specific questions. Do cells survive for substantial periods after whole-cell recording *in vivo*? What is the likelihood and longevity of whole-cell recordings with internal solutions containing plasmid DNA? Can plasmid DNA dialyze into the cell and drive protein expression? Is protein expression restricted to the patched cell?

After demonstrating the feasibility of this approach, we highlight its potential by recording the synaptic responses of neurons in mouse primary visual cortex to presentation of drifting gratings while delivering vectors to allow monosynaptic retrograde labeling using a modified rabies virus[23]. Several days after virus injection we observed unprecedented numbers of labeled neurons, which made it possible for us to register a cell's synaptic receptive field and the presynaptic cells that define it.

RESULTS

Recovery rates of *in vivo* whole-cell recorded neurons

It is generally assumed that whole-cell recording substantially compromises cell viability. Therefore, when morphological confirmation is required after *in vivo* whole-cell recording, animals are usually killed immediately and the tissue fixed for histological analysis[29]. We directly tested this assumption by performing *in vivo* whole-cell recordings from cells in layers 2–5 of mouse neocortex using a biocytin-containing intracellular solution and assessing the incidence and morphology

[1]Department of Neuroscience, Physiology and Pharmacology, University College London, London, UK. [2]Division of Neurophysiology, The National Institute for Medical Research, Mill Hill, UK. [3]Department of Neuroscience, Columbia University, New York, New York, USA. [4]Department of Molecular Neurobiology, Max Planck Institute for Medical Research, Heidelberg, Germany. [5]SNWG Behavioural Neurophysiology, Max Planck Institute for Medical Research, Heidelberg, Germany. [6]These authors contributed equally to this work. Correspondence should be addressed to T.W.M. (troy.margrie@nimr.mrc.ac.uk).

Received 26 October 2010; accepted 18 January 2011; published online 20 February 2011; doi:10.1038/nn.2765

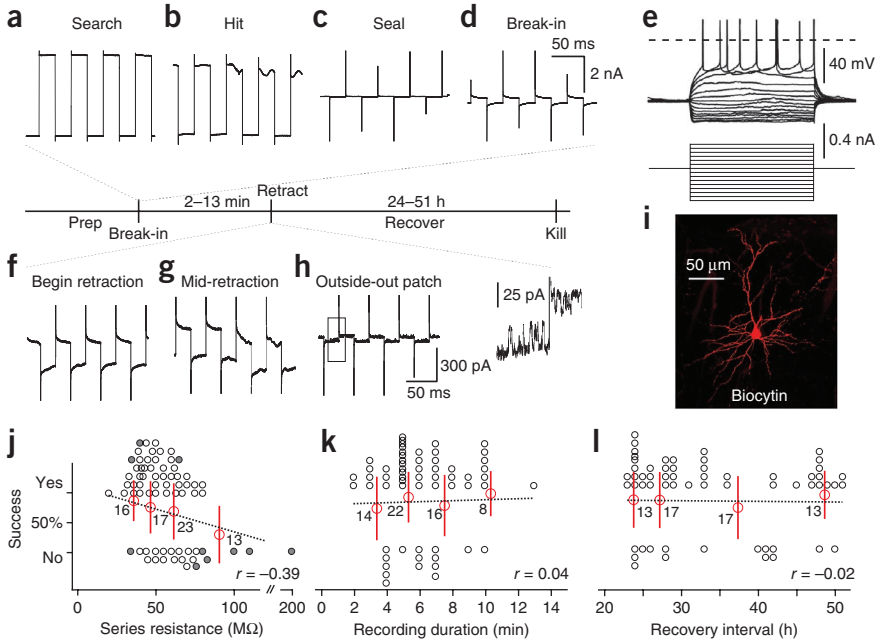

Figure 1 Recording methodology and biocytin recovery rates. (**a**) Seal test current trace used to monitor pipette resistance. (**b**) Contact with cell membrane while stepping the electrode indicated by rhythmic changes in pipette resistance associated with heartbeat-related movement. (**c**,**d**) Traces showing seal formation (**c**) and whole-cell access (**d**). (**e**) Current-voltage relationship (current injections 50-pA steps for 600 ms) recorded from the cell shown in **i**. (**f**–**h**) Current traces in response to voltage steps immediately before (**f**) and during pipette retraction (**g**) to achieve the outside-out patch configuration (**h**). Inset trace: detail from **h** showing single-channel currents. (**i**) Example morphology of a biocytin-labeled layer 2/3 pyramidal cell (mouse terminated 29 h after recording). (**j**) Success rates of biocytin-filled cell recovery plotted against series resistance of recording (determined within 30 s of break-in). Open circles represent, on a cell-by-cell basis, recovery success or failure. Gray-filled circles indicate those recordings that did not meet retraction or series resistance criteria. Large open red circles represent the mean success for each bin (ranges: 20–40, 41–50, 53–70, 71–200 MΩ). All error bars show s.d. Numbers indicate *n* for each bin. Dashed lines are linear fits to the individual data points. (**k**,**l**) Success rates of cell recovery plotted against duration of recording (**k**; bin ranges: 1–4, 5–6, 7–9, 10–13 min) and the interval between recording and terminating the mouse (**l**; bin ranges: 23–24, 25–29, 31–45, 47–51 h).

of labeled neurons several days after recording. The method for obtaining whole-cell recordings was essentially as described[14]. Briefly, we filled a glass electrode with a potassium-based intracellular solution and advanced it quickly to the target depth under moderate positive pressure (**Fig. 1a**). We then reduced the positive pressure and advanced the electrode while monitoring the tip resistance. We removed the pressure upon 'hitting' a cell, judged by changes in the tip resistance (**Fig. 1b**), and applied negative pressure to help with seal formation (**Fig. 1c**). We achieved whole-cell access by brief bursts of negative pressure to rupture the cell membrane (**Fig. 1d**). In the whole-cell configuration and in current-clamp mode, we recorded the current-voltage relationship (**Fig. 1e**) and spontaneous and evoked activity. At the end of the recording we slowly withdrew the patch pipette while constantly monitoring the access resistance in voltage-clamp mode (**Fig. 1f**,**g**). Pipette retraction usually resulted in membrane resealing (**Fig. 1g**) and formation of an outside-out patch (**Fig. 1h**) that was considered an important, though not essential, predictor of cell recovery. After whole-cell recording, we allowed mice to recover and returned them to their home cages (see Online Methods).

To assess the survival rate of recorded neurons, we terminated mice 24–51 h after recording, removed and fixed the brain and prepared slices (see Online Methods). Most of the recorded cells were pyramidal cells and their recovered morphologies typically included an apical dendrite that extended up to layer 1 (**Fig. 1i**). The morphological criterion for classifying cells as recovered was that the cell soma and the proximal regions of at least four dendrites were visible. The number of recovered cells per brain that met this criterion never exceeded the number of cells recorded.

Our criteria for considering recorded cells as being potentially recoverable included that the initial series resistance was below 80 MΩ (**Fig. 1j**). In most cases (>90%), these recordings were actively terminated as described above (**Fig. 1**). In 10 cases where the retraction criterion was not met or series resistance was more than 80 MΩ, we successfully carried out another recording in the same animal at a different cortical depth. In these cases we recovered 3/10 cells in which recordings did not satisfy both criteria (**Fig. 1j**). Cells that did not meet these criteria have not been further included. We found that parameters such as recording duration (up to 13 min) and recovery interval (up to 51 h) did not correlate with the likelihood of observing biocytin-filled cells (**Fig. 1k**,**l**). According to these criteria, we recovered 78% (47/60) of recorded cells after biocytin visualization with Atto-565- or Alexa-488-conjugated streptavidin (**Fig. 1i**). This indicates that neurons can reliably survive whole-cell recording and maintain their structural integrity.

Recording with internal solutions containing plasmid DNA

To determine the feasibility of DNA loading during whole-cell recording, we performed recordings with intracellular solutions containing up to 350 ng μl^{-1} of plasmid DNA encoding fluorescent proteins (see Online Methods) and biocytin. Qualitatively, the likelihood of obtaining seals and low-resistance recordings with internal solutions containing DNA was similar to that found using standard internal solutions.

Cells recorded with plasmid DNA in the pipette had firing profiles typical of cortical neuronal subclasses[15,29,30] (**Fig. 2a**). Stable resting membrane potentials, ongoing synaptic activity (**Fig. 2b**) and overshooting action potentials (**Fig. 2b**) indicated that cells remained healthy for the duration of the recording (up to 13 min). All recordings were actively terminated after the intrinsic biophysical properties (**Fig. 2a**) and synaptic receptive fields of cells had been obtained (**Fig. 2c**,**d**).

After slowly retracting the pipette, we allowed the mice to recover for at least 24 h (range 24–51 h) before perfusing them. Usually we recorded only one cell per animal, though in some mice several cells (typically two) were recorded in different layers, allowing electrophysiology and GFP fluorescence to be unambiguously matched. All recordings for these experiments were actively and successfully terminated.

Protein expression

We often recovered intensely fluorescent cells, which were always in the expected locations and had elaborate dendritic morphologies consistent with predictions from electrophysiological data (**Fig. 2a**,**b**). Of the 39 cells recorded with internal solution containing DNA, 22 to expressed GFP. In all cases where we found GFP-labeled cells (within 51 h of recording), cells were also positive for biocytin (**Fig. 2e**). However, nine cells were biocytin-positive and did not express GFP. After immunohistochemical amplification, GFP-positive cells always contained label in dendritic spines and axons (**Fig. 2f**). Unlike the biocytin label, we observed expression of the fluorescent protein only in single cells and never along the electrode tract (**Fig. 2e**). In recordings in which the internal solution contained DNA, series resistance had a similar effect on recovery probability as with recordings with biocytin (**Fig. 2g**); recording duration and recovery interval seemed to have no effect (**Fig. 2h**,**i**). Thus, after whole-cell recording with plasmid-containing intracellular solution, 56% of cells expressed fluorescent protein specifically in and only in the recorded cell.

The delivery of multiple genes into a specific neuron that has been electrophysiologically characterized has obvious advantages. We therefore investigated whether multiple vectors could be reliably co-expressed by including two or three types of plasmid encoding proteins that fluoresce at different wavelengths (for example, td-Tomato, Cerulean and Venus) in our intracellular solution. For experiments using multiple plasmids, 3/7 cells were recovered, and fluorescence was observed at all appropriate wavelengths in all recovered cells (**Fig. 3a**,**b**).

These results show that neurons can survive *in vivo* whole-cell recordings. DNA plasmids in the intracellular solution do not impair the electrophysiological characterization of cells but readily dialyze into the neuron and cause the expression of exogenous genes. As plasmid DNA expelled into the extracellular space is not expressed, transfection is restricted to the recorded cell. This method therefore seems to be ideally suited to span neurophysiological and genetic approaches for understanding the function of specific cells and circuits *in vivo*.

Application: bridging single-cell function and connectivity

The monosynaptic control of the spread of modified rabies virus into presynaptic neurons has been reported[23]. It is accepted that the native, non-modified rabies virus infects synaptically connected neurons exclusively in the retrograde direction[31,32] and that this process relies on the rabies virus glycoprotein (RV-G)[33,34]. When the RV-G gene is deleted and replaced by a gene that encodes a fluorescent protein, the modified rabies virus is rendered incompetent for trans-synaptic infection but can replicate inside the initially infected cell. Infection by RV-G–deficient rabies virus encapsulated with the avian sarcoma and leucosis virus envelope protein (*SAD-ΔG-mCherry-EnvA*) is restricted to those cells that express an avian receptor protein (TVA) that is not expressed in mammals. Thus, if a single cell is transfected with vectors expressing TVA and RV-G, only this cell will be susceptible to initial infection and provide the incompetent virus with the RV-G required for trans-synaptic infection. The virus can therefore spread from the primarily infected cell to its presynaptic inputs and express fluorescent protein in these cells. However, as RV-G is not expressed in the presynaptic cells, the virus can spread no further. This approach therefore labels only first-order neurons that are presynaptically connected to the primary cell[23,26,32].

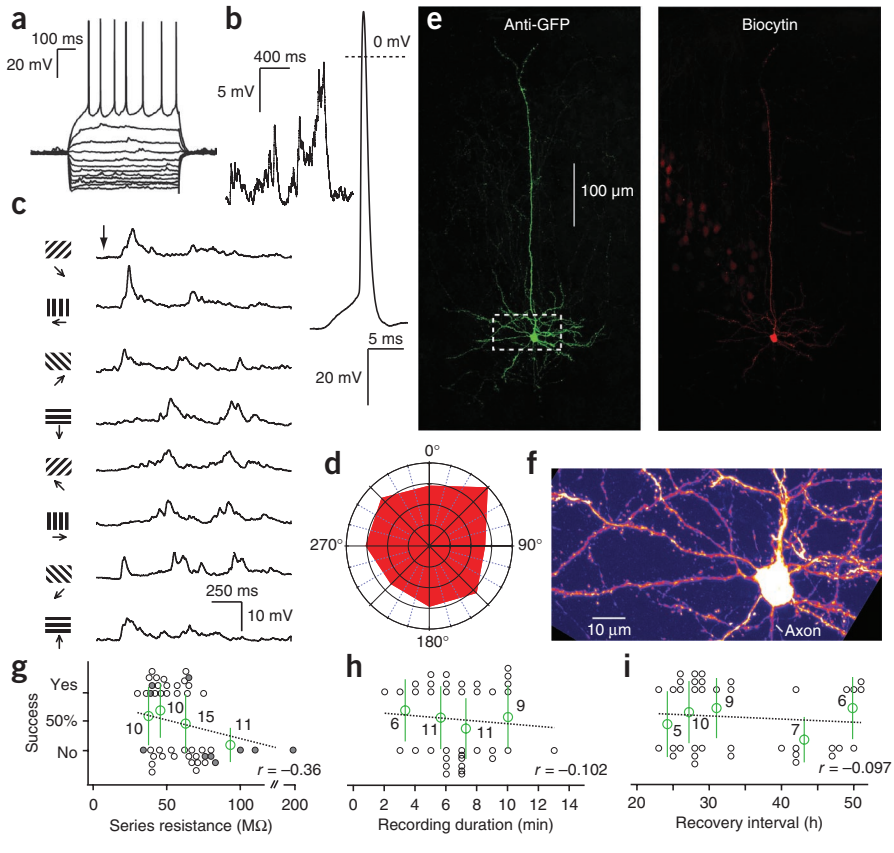

Figure 2 Physiological characterization and genetic manipulation. (**a**) The firing profile and current-voltage relationship recorded from the layer 5 neuron shown in **e**. Voltage traces shown are in response to 50-pA current steps of 600-ms duration. (**b**) Membrane voltage traces showing spontaneous synaptic activity and the kinetics of a resultant action potential. (**c**) Synaptic responses (average of ten sweeps) to drifting gratings moving in the direction indicated by the arrows (left). Arrow (top) indicates onset of grating drift. (**d**) Polar plot showing integral of the membrane voltage traces (for 1,400 ms from stimulus onset). (**e**) Layer 5 pyramidal cell in primary visual cortex 26 h after recording showing GFP expression (left) and biocytin labeling (right). Note the weak, non-specific biocytin signal along the electrode track due to the plume of biocytin expelled while approaching the recorded cell. (**f**) GFP signal in dendritic spines and axonal arborizations in the same cell. (**g**) Success rates of GFP-labeled cell recovery plotted against series resistance of recording (determined within 30 s of break-in). Open circles represent, on a cell-by-cell basis, recovery success or failure. Gray-filled circles are cases that did not meet retraction or series resistance criteria. Open green circles represent the mean success for each bin (ranges: 20–40, 41–50, 53–70, 71–200 MΩ). All error bars show s.d. Numbers indicate *n* for each bin. Dashed lines are linear fits to the individual data points. (**h**,**i**) Success rates of cell recovery plotted against duration of recording (**h**; bin ranges: 1–4, 5–6, 7–8, 9–13 min) and the interval between recording and terminating each mouse (**i**; bin ranges: 23–25, 26–28, 29–33, 40–47, 48–51 h).

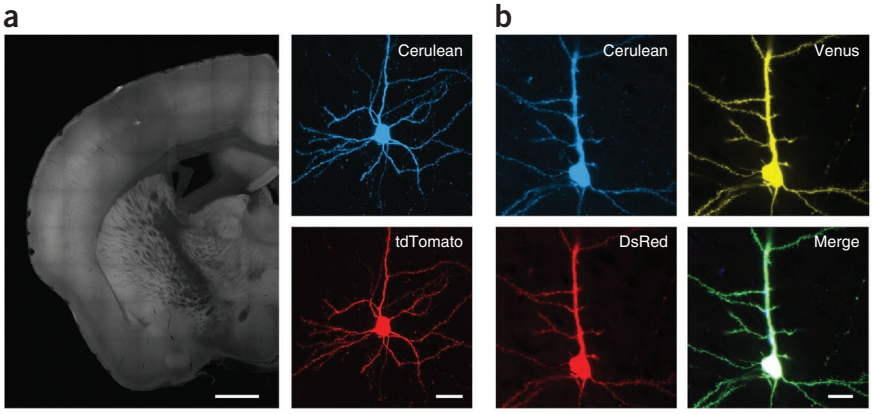

Figure 3 Multiple gene delivery. (**a**) Native fluorescence images of a layer 5 neuron in somatosensory cortex 3 d after patching with *pCAGGS-Cerulean* (top right) and *pCAGGS-tdTomato* (50 ng μl^{-1} each, bottom right). Scale bars, 824 µm (left) and 20 µm (right). (**b**) Gallery of native fluorescence images for a layer 2/3 cell in somatosensory cortex 5 d after recording with *pCAGGS-DsRed2*, *pCAGGS-Venus* and *pCAGGS-ChR2-Cerulean*. Scale bar, 20 µm.

To show the potential of genetic manipulation by whole-cell recording *in vivo* to bridge our understanding of cell function and connectivity we first recorded the intrinsic properties (**Fig. 4a**) and visually evoked synaptic responses (**Fig. 4b**) of layer 5 pyramidal cells in mouse visual cortex (n = 8) to drifting gratings of different orientations (see Online Methods). Synaptic responses were more broadly tuned than spiking output but showed similar orientation preferences[35,36] (**Fig. 4b**,**c**). Furthermore, the evoked synaptic activity fluctuated substantially during such responses in an orientation-specific manner (**Fig. 4c**). During functional characterization we simultaneously delivered a vector that directed expression of both the TVA receptor and RV-G, and a second vector that directed expression of GFP (**Fig. 4d**,**e**). We injected ~200 nl of *SAD-ΔG-mCherry-EnvA* into layer 5 2 d after recording.

Between 4 and 13 d after injection we transcardially perfused the mice (n = 8) and prepared 100- or 200-µm-thick brain slices (see Online Methods). We then imaged fluorescent signals using confocal microscopy[37]. In three of the eight mice, we observed hundreds of mCherry-expressing neurons (n = 152, 221 and 666; **Fig. 4d–g** and **Supplementary Fig. 1**) in and outside of primary visual cortex. In two of the remaining five mice, we observed a single GFP-expressing cell but no mCherry signal, probably indicating successful transfection in cells that were not subsequently infected with the pseudotyped rabies virus. In the remaining three mice we could not detect cells expressing either GFP or mCherry. In control animals (n = 2) that received only virus

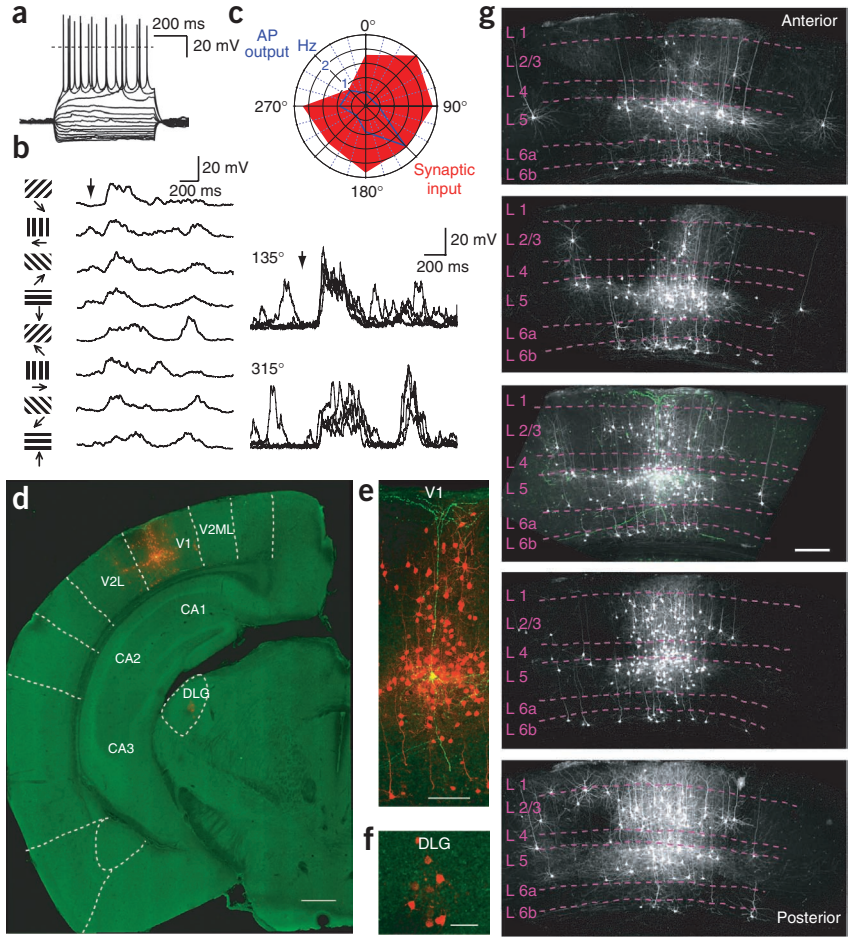

Figure 4 Synaptic receptive mapping and connectivity of a visual cortical neuron. (**a**) Firing profile and current-voltage relationship recorded from the GFP-expressing cell shown in **d**. Voltage traces shown are in response to 50-pA current steps of 600-ms duration. (**b**) Synaptic responses (average of ten sweeps) to drifting gratings moving in the direction indicated by the arrows (left). Arrow (top) indicates onset of drift. Current injection (–200 pA) was delivered to isolate evoked synaptic responses from action potential activity. (**c**) Polar plot showing integral of the voltage traces (red) recorded during the duration of the drifting grating. The integral of synaptic responses (1,400 ms from stimulus onset) are normalized to the largest response. Below are five example traces recorded for the least and most preferred orientations. For the spiking receptive field (blue), holding current was removed and the stimulus sequence (**b**) was repeated five times. (**d**) Coronal slice (100 µm thick) showing anti-GFP (green) and anti-RFP (red) fluorescence. The recorded layer 5 neuron (green-yellow) in primary visual cortex (V1) and mCherry-labeled cells (red) are clearly identifiable. In this slice we observed ~200 presynaptic cells. Scale bar, 500 µm. Abbreviations: V2ML: secondary visual cortex mediolateral; V2L: secondary visual cortex lateral; CA1–3: hippocampal fields CA1–3; DLG: dorsolateral geniculate nucleus. (**e**) High-magnification image showing GFP and mCherry labeled cells in V1. Scale bar, 100 µm. (**f**) Eight mCherry-labeled cells in the DLG. Scale bar, 50 µm. (**g**) Five maximum intensity projections for consecutive 100-µm-thick slices. The middle panel contains the host cell (green; scale bar, 200 µm). This mouse was killed 7 d after virus injection (9 d after recording).

injection (500 nl) we observed six mCherry-positive glia and one neuron (**Supplementary Fig. 1**). These data show that by combining *in vivo* whole-cell transfection with trans-synaptic tracing methods it is possible to record the synaptic receptive fields of neurons while delivering the genetic machinery that is needed to identify the presynaptic cells whose activity underlie such receptive fields.

DISCUSSION

Here we have shown that the whole-cell patch clamp method can be used to transfect single cells during neuronal recording *in vivo*. Perhaps the most unexpected aspect of our results is the high neuronal survival rate after *in vivo* whole-cell recording. This finding is consistent with a study in which neurons in acute cortical slices were patched and then re-patched up to 12 h later, and remained healthy although their connectivity could be altered[38]. Here, we have investigated cell mortality *in vivo* up to 51 h after recording using morphological criteria. Consistent with data obtained from slices, the large number of healthy neurons observed after *in vivo* recording ensures that the likelihood of genetic manipulation is relatively high (~50%). We found that, following transfection, neurons remained viable, as they continued to express reporter proteins for up to 1 week.

The delivery of DNA into neurons through an intracellular recording method should be considered useful for any experimental system including neuronal and non-neuronal cultures where cells can be maintained for extended periods of time. In combination with electrical recording from the cell, the list of potential applications of this method includes genetic perturbation of intracellular signaling cascades and up- or downregulation of ion channels, membrane receptors, light-activatable ion channels or genetically encoded indicators, expressed across functionally related presynaptic circuits.

Series resistance seems to be the most important factor influencing the recovery rate of both biocytin-filled and DNA-loaded cells. This is consistent with evidence that the efficiency of loading substances such as dyes and biocytin is reduced as series resistance increases[28]. As with dye loading, the relatively low access resistance of intracellular recordings obtained with the patch pipettes used *in vivo* are suitable for DNA delivery. When we recovered cells from which we had recorded with intracellular solutions containing multiple reporter plasmids, we always observed all of the expected fluorescent proteins (up to three). Though we have not established an upper limit, this suggests that our transfection approach results in the reliable delivery of multiple plasmids. Given that plasmids can contain more than one protein-encoding sequence, a substantial number of genes could be delivered simultaneously by this method.

Genetic manipulation through electroporation has been complemented with two-photon imaging to allow targeted gene delivery to single neurons in the mouse brain[26], with similar success rates to those reported here. Although such a targeted electroporation method is promising, its application is limited. Specifically, although action potentials in the target cell could, in principle, be detected[39] before electroporation, cell-attached recordings are highly restricted since they preclude measurements of synaptic and intrinsic properties. Second, successful single-cell *in vivo* electroporation has required visualization[26,40,41], limiting this method to optically accessible structures in the intact brain. Although the whole-cell transfection method described here can be combined with optical monitoring to target specific cell types[30,41], we have used blind whole-cell recordings for single-cell transfection in optically inaccessible, deeper structures[14–18]. It therefore appears that any cell type that can be patched can be genetically modified in the process.

Here we used modified rabies virus-mediated monosynaptic retrograde tracing to demonstrate one application of combined whole-cell recording and multi-gene delivery. During recording of intrinsic properties and visually evoked synaptic responses we delivered genes to direct the infection and spread of *SAD-ΔG-mCherry-EnvA* in the recorded cell. The resulting number of mCherry-labeled cells presynaptic to layer 5 neurons shown here substantially exceeds that for layer 2/3 cells observed in a recent electroporation study[26]. This disparity might reflect differences between the connectivity of layer 2/3 and layer 5 pyramidal neurons. However, the difference in the extent of presynaptic labeling might also reflect differences in the efficiency of plasmid delivery and protein expression between these two methods.

Wild-type rabies virus has long been used as a reliable retrograde trans-neuronal tracer[32]. By combining whole-cell recording and DNA delivery with retrograde tracing using modified rabies virus we have determined both the physiological properties and connectivity profile of a single neuron. By further combining this with either bolus loading of calcium dyes[42] or using virus-mediated genetically driven expression of calcium indicators[43–45] it will be possible to implement *in vivo* two-photon-based population imaging[2,42,46,47] (at least of cells in upper cortical layers) to investigate temporal correlations of firing of known presynaptic cells and the unique synaptic responses recorded from the postsynaptic neuron. It will be interesting, for example, to investigate whether commonalities in connectivity reflect any bias in function.

Only by probing both the function and connectivity of specific cells and circuits can we obtain a complete understanding of the functional architecture of the brain[27]. The method of DNA delivery by whole-cell recording described here provides a versatile tool for both assaying and manipulating single cells and probing the functional connectivity of specific local and long-range networks.

METHODS

Methods and any associated references are available in the online version of the paper at http://www.nature.com/natureneuroscience/.

Note: Supplementary information is available on the Nature Neuroscience website.

ACKNOWLEDGMENTS

K.M.F. thanks S. Siegelbaum and R. Axel for support and encouragement and A. Mulligan for technical assistance. We also thank P.H. Seeburg for support; D. Castro, B. Matynoga and D. Drechsel for advice; K.-K. Conzelmann for rabies virus *SAD-ΔG-mCherry*; and P. Boross, E. Callaway, H. Wildner and F. Guillemot for discussions and reagents. E.A.R. is a Sir Henry Wellcome Postdoctoral Fellow. This work was supported by The Robert Leet and Clara Guthrie Patterson Trust and a National Institute on Deafness and Other Communication Disorders (NIDCD) K99 grant (K.M.F.), The Max-Planck Gesellschaft (A.T.S., M.K.S.), the Medical Research Council (MRC) and The Alexander Von Humboldt Foundation (T.W.M.).

AUTHOR CONTRIBUTIONS

E.A.R., K.M.F., A.T.S. and T.W.M. conceived experiments. K.M.F., A.T.S. and T.W.M. performed original proof-of-principle and multi-plasmid experiments. E.A.R. collected the biocytin, GFP and viral tracing data. M.K.S. co-designed and generated plasmids and provided virus. B.P. provided customized visual stimulation and compiled large-scale imaging data. E.A.R., K.M.F. and T.W.M. wrote the manuscript with input from all other authors.

COMPETING FINANCIAL INTERESTS

The authors declare no competing financial interests.

Published online at http://www.nature.com/natureneuroscience/.
Reprints and permissions information is available online at http://npg.nature.com/reprintsandpermissions/.

1. Kleinfeld, D. & Griesbeck, O. From art to engineering? The rise of *in vivo* mammalian electrophysiology via genetically targeted labeling and nonlinear imaging. *PLoS Biol.* **3**, e355 (2005).

2. Helmchen, F. & Denk, W. Deep tissue two-photon microscopy. *Nat. Methods* **2**, 932–940 (2005).
3. Luo, L., Callaway, E.M. & Svoboda, K. Genetic dissection of neural circuits. *Neuron* **57**, 634–660 (2008).
4. Arenkiel, B.R. & Ehlers, M.D. Molecular genetics and imaging technologies for circuit-based neuroanatomy. *Nature* **461**, 900–907 (2009).
5. Geschwind, D.H. & Konopka, G. Neuroscience in the era of functional genomics and systems biology. *Nature* **461**, 908–915 (2009).
6. O'Connor, D.H., Huber, D. & Svoboda, K. Reverse engineering the mouse brain. *Nature* **461**, 923–929 (2009).
7. Scanziani, M. & Hausser, M. Electrophysiology in the age of light. *Nature* **461**, 930–939 (2009).
8. Gradinaru, V. *et al.* Molecular and cellular approaches for diversifying and extending optogenetics. *Cell* **141**, 154–165 (2010).
9. Lichtman, J.W., Livet, J. & Sanes, J.R. A technicolour approach to the connectome. *Nat. Rev. Neurosci.* **9**, 417–422 (2008).
10. Margrie, T.W., Sakmann, B. & Urban, N.N. Action potential propagation in mitral cell lateral dendrites is decremental and controls recurrent and lateral inhibition in the mammalian olfactory bulb. *Proc. Natl. Acad. Sci. USA* **98**, 319–324 (2001).
11. Wehr, M. & Zador, A.M. Balanced inhibition underlies tuning and sharpens spike timing in auditory cortex. *Nature* **426**, 442–446 (2003).
12. Waters, J., Larkum, M., Sakmann, B. & Helmchen, F. Supralinear Ca2+ influx into dendritic tufts of layer 2/3 neocortical pyramidal neurons *in vitro* and *in vivo*. *J. Neurosci.* **23**, 8558–8567 (2003).
13. Loewenstein, Y. *et al.* Bistability of cerebellar Purkinje cells modulated by sensory stimulation. *Nat. Neurosci.* **8**, 202–211 (2005).
14. Margrie, T.W., Brecht, M. & Sakmann, B. *In vivo* whole-cell recordings from neurons in the anaesthetized and awake mammalian brain. *Pflügers Arch.* **444**, 491–498 (2002).
15. Brecht, M., Schneider, M., Sakmann, B. & Margrie, T.W. Whisker movements evoked by stimulation of single pyramidal cells in rat motor cortex. *Nature* **427**, 704–710 (2004).
16. Arenz, A., Silver, R.A., Schaefer, A.T. & Margrie, T.W. The contribution of single synapses to sensory representation *in vivo*. *Science* **321**, 977–980 (2008).
17. Harvey, C.D., Collman, F., Dombeck, D.A. & Tank, D.W. Intracellular dynamics of hippocampal place cells during virtual navigation. *Nature* **461**, 941–946 (2009).
18. Epsztein, J., Lee, A.K., Chorev, E. & Brecht, M. Impact of spikelets on hippocampal CA1 pyramidal cell activity during spatial exploration. *Science* **327**, 474–477 (2010).
19. Hromádka, T., Deweese, M.R. & Zador, A.M. Sparse representation of sounds in the unanesthetized auditory cortex. *PLoS Biol.* **6**, e16 (2008).
20. Lee, A.K., Epsztein, J. & Brecht, M. Head-anchored whole-cell recordings in freely moving rats. *Nat. Protoc.* **4**, 385–392 (2009).
21. Zhang, F., Aravanis, A.M., Adamantidis, A., de Lecea, L. & Deisseroth, K. Circuit-breakers: optical technologies for probing neural signals and systems. *Nat. Rev. Neurosci.* **8**, 577–581 (2007).
22. Zhang, F., Wang, L.-P., Boyden, E.S. & Deisseroth, K. Channelrhodopsin-2 and optical control of excitable cells. *Nat. Methods* **3**, 785–792 (2006).
23. Wickersham, I.R. *et al.* Monosynaptic restriction of transsynaptic tracing from single, genetically targeted neurons. *Neuron* **53**, 639–647 (2007).
24. Huber, D. *et al.* Sparse optical microstimulation in barrel cortex drives learned behaviour in freely moving mice. *Nature* **451**, 61–64 (2008).
25. Komai, S. *et al.* Postsynaptic excitability is necessary for strengthening of cortical sensory responses during experience-dependent development. *Nat. Neurosci.* **9**, 1125–1133 (2006).
26. Marshel, J.H., Mori, T., Nielsen, K.J. & Callaway, E.M. Targeting single neuronal networks for gene expression and cell labeling *in vivo*. *Neuron* **67**, 562–574 (2010).
27. Douglas, R.J. & Martin, K.A. Mapping the matrix: the ways of neocortex. *Neuron* **56**, 226–238 (2007).
28. Eilers, J.K. & Konnerth, A. A practical guide: dye loading with patch pipettes. in *Imaging in Neuroscience and Development* (eds. Yuste, R.K. & Konnerth, A.) 277–281 (Cold Spring Harbor Laboratory Press, Cold Spring Harbor, New York, 2005).
29. Brecht, M. *et al.* Organization of rat vibrissa motor cortex and adjacent areas according to cytoarchitectonics, microstimulation, and intracellular stimulation of identified cells. *J. Comp. Neurol.* **479**, 360–373 (2004).
30. Margrie, T.W. *et al.* Targeted whole-cell recordings in the mammalian brain *in vivo*. *Neuron* **39**, 911–918 (2003).
31. Ugolini, G. Specificity of rabies virus as a transneuronal tracer of motor networks: transfer from hypoglossal motoneurons to connected second-order and higher order central nervous system cell groups. *J. Comp. Neurol.* **356**, 457–480 (1995).
32. Ugolini, G. Advances in viral transneuronal tracing. *J. Neurosci. Methods* **194**, 2–20 (2010).
33. Mebatsion, T., Konig, M. & Conzelmann, K.K. Budding of rabies virus particles in the absence of the spike glycoprotein. *Cell* **84**, 941–951 (1996).
34. Mebatsion, T. Extensive attenuation of rabies virus by simultaneously modifying the dynein light chain binding site in the P protein and replacing Arg333 in the G protein. *J. Virol.* **75**, 11496–11502 (2001).
35. Ferster, D. Origin of orientation-selective EPSPs in simple cells of cat visual cortex. *J. Neurosci.* **7**, 1780–1791 (1987).
36. Mariño, J. *et al.* Invariant computations in local cortical networks with balanced excitation and inhibition. *Nat. Neurosci.* **8**, 194–201 (2005).
37. Conchello, J.-A. & Lichtman, J.W. Optical sectioning microscopy. *Nat. Methods* **2**, 920–931 (2005).
38. Le Bé, J.V. & Markram, H. Spontaneous and evoked synaptic rewiring in the neonatal neocortex. *Proc. Natl. Acad. Sci. USA* **103**, 13214–13219 (2006).
39. de Kock, C.P. & Sakmann, B. Spiking in primary somatosensory cortex during natural whisking in awake head-restrained rats is cell-type specific. *Proc. Natl. Acad. Sci. USA* **106**, 16446–16450 (2009).
40. Nevian, T. & Helmchen, F. Calcium indicator loading of neurons using single-cell electroporation. *Pflügers Arch.* **454**, 675–688 (2007).
41. Kitamura, K., Judkewitz, B., Kano, M., Denk, W. & Hausser, M. Targeted patch-clamp recordings and single-cell electroporation of unlabeled neurons *in vivo*. *Nat. Methods* **5**, 61–67 (2008).
42. Stosiek, C., Garaschuk, O., Holthoff, K. & Konnerth, A. *In vivo* two-photon calcium imaging of neuronal networks. *Proc. Natl. Acad. Sci. USA* **100**, 7319–7324 (2003).
43. Tian, L. *et al.* Imaging neural activity in worms, flies and mice with improved GCaMP calcium indicators. *Nat. Methods* **6**, 875–881 (2009).
44. Mank, M. *et al.* A genetically encoded calcium indicator for chronic *in vivo* two-photon imaging. *Nat. Methods* **5**, 805–811 (2008).
45. Lutcke, H. *et al.* Optical recording of neuronal activity with a genetically-encoded calcium indicator in anesthetized and freely moving mice. *Front. Neural Circuits* **4**, 9 (2010).
46. Ohki, K., Chung, S., Ch'ng, Y.H., Kara, P. & Reid, R.C. Functional imaging with cellular resolution reveals precise micro-architecture in visual cortex. *Nature* **433**, 597–603 (2005).
47. Rochefort, N.L. *et al.* Sparsification of neuronal activity in the visual cortex at eye-opening. *Proc. Natl. Acad. Sci. USA* **106**, 15049–15054 (2009).

ONLINE METHODS

Intracellular solutions. Intracellular solutions for whole-cell recordings were made up in concentrated stock (1.2–3 times the final concentration) to allow plasmid addition. The final concentrations were (in mM, all from Sigma-Aldrich or VWR International) 130 K-methanesulphonate, 10 Hepes, 7 KCl, 0.05 EGTA, 2 Na_2ATP, 2 MgATP, 0.5 Na_2GTP; pH was adjusted to 7.28 using KOH. The final osmolarity after adding 0.5% biocytin (wt/wt) or suspended plasmids was adjusted to 280–290 mOsm. Intracellular solutions were filtered through a 0.2-µm pore size syringe filter (Whatman) or a 0.22-µm pore size centrifuge filter (Costar Spin-X). Spectrophotometry (NanoDrop 1000, Thermo Scientific) showed that DNA was not lost during filtration.

Plasmid production. The coding sequences of DsRed2, tdTomato, Venus, Cerulean or ChR2-Cerulean were subcloned into *pCAGGS*. For GFP we used *pCA-b-GFPm5 silencer 3* (gift from H. Wildner and F. Guillemot). For rabies virus–mediated transneuronal tracing, coding sequences of rabies RV-G and TVA (ref. 23) were linked with an internal ribosomal entry site (IRES2, DB Biosciences) and sub-cloned into *pCA-b-GFPm5 silencer 3* by replacing the GFP coding sequence. Correct insertion and coding sequences were verified by subsequent DNA sequencing. Resulting plasmids were transformed and individual clones were grown in *Escherichia coli* Stbl3 (Invitrogen) cells to avoid recombination. DNA for *in vivo* recordings was prepared using an endotoxin-free maxiprep kit (Qiagen) and suspended in ultrapure H_2O or TE buffer (Qiagen). Plasmid aliquots (10 µl) were diluted in H_2O and added to the intracellular solution for a final concentration of ~50–350 ng $µl^{-1}$.

Production of pseudotyped rabies virus. BHK cells were plated at a density of ~1.5×10^7. The next day, cells were transfected with 15 µg plasmid *pCAG-G (SAD-G)* (gift from K.-K. Conzelmann, Max-von-Pettenkofer Institute) by CaP transfection. After 24 h rabies virus *SAD-ΔG–mCherry* was added at a multiplicity of infection (MOI) of 3. After another 48 h the *SADΔG-mCherry* containing supernatant was equally distributed onto four 15-cm plates containing *pCAG-G (SAD-G)* (15 µg per plate)-transfected BHK cells (~1.5×10^7 cells per plate). Two days later the virus-containing supernatant was applied onto four - plates containing BHK-EnvARGCD cells[23] (~1.5×10^7 cells per plate) at an MOI of 1.5 for pseudotyping. Twelve hours later cells were trypsinized and replated onto eight 15-cm dishes. Pseudotyped rabies virus-containing supernatant was harvested 2 d later. The supernatant was spun at 2,000 rpm at 4 °C for 10 min and subsequently filtered through a 0.45-µm filter. The filtered virus suspension was centrifuged for 90 min at 25,000 rpm (SW28, 4 °C) in a Beckmann 80K ultracentrifuge. After centrifugation the supernatant was discarded and the pellet was aspirated in phosphate buffered saline solution (PBS, Sigma Aldrich). Solution containing pseudotyped rabies virus was aliquoted in 10-µl aliquots and frozen at −70 °C. Virus titers (~2.5×10^7 ml^{-1}) were determined by serial dilution and overnight infection of primary cortical neurons that had been infected with rAAV1/2-expressing *TVA-IRES-GFP*[23] under the control of the human synapsin promoter/enhancer[48]. Three days later the number of red fluorescent, *SAD-ΔG–mCherry*–containing neurons was counted.

Surgical procedures. Young adult C57/BL6 mice (4–6 weeks old) were anaesthetized with a mixture of ketamine and xylazine (100 mg kg^{-1} and 10 mg kg^{-1}, respectively) injected intraperitoneally, supplemented as necessary whenever the animal showed toe-pinch reflexes. Mice were head-fixed using non-puncture ear-bars and a nose-clamp (SG-4N, Narishige), and their body temperature maintained at 36–37 °C using a rectal probe and a heating blanket (FHC). An incision was made in the scalp and a small craniotomy was drilled above the relevant area of cortex using a dental drill (Osada Electric Co) and the dura removed. The surface of the brain was kept moist by applying sterile PBS at regular intervals. Following recordings, the craniotomy was sealed using a silicone sealant (Kwik-Sil, World Precision Instruments) and the scalp sutured. The wound was infiltrated with lidocaine and a topical antibiotic (Cicatrin, GlaxoSmithKline) was applied. The time from the initial anaesthesia to completing this procedure was kept as short as possible (<2 h). During recovery, mice were kept warm in a heating box (Harvard Apparatus) for 3–4 h under constant observation. All procedures were approved by the local ethics panel and UK Home Office under the Animals (Scientific Procedures) Act 1986.

Obtaining whole-cell recording. *In vivo* whole-cell recordings were carried out as described[14]. Briefly, glass electrodes were pulled from borosilicate glass (GC150F, Harvard Apparatus Ltd) on a vertical puller (PC-10, Narishige) to a tip resistance of 6–7 MΩ. Recordings were carried out with an AxoClamp 2B or Mulitclamp 700B amplifier (Axon Instruments). Data were filtered at 3 kHz and digitized at 10–20 kHz using an ITC-18 A/D-D/A interface (InstruTECH, Heka Elektronik) and the Neuromatic package (http://www.neuromatic.thinkrandom.com/) under Igor Pro 5 (http://www.wavemetrics.com/).

Discontinuation of whole-cell recording. After recording, the patch pipette was slowly withdrawn (~3 µm s^{-1}) while the seal test pulse was monitored in voltage-clamp mode to determine access resistance. Often this resulted in pulling an outside-out patch of membrane, which we consider to be an important but not essential criterion for cell survival. The electrical access to the cell could also be monitored by shifts in holding current due to ongoing synaptic input and in some cases the occurrence of unclamped action currents. Applying a quick negative pressure pulse to abruptly break the seal with no indication of action currents indicated successful outside-out patch formation.

Synaptic receptive field mapping. Visual stimuli were generated using Matlab (Mathworks) and Psychophysics Toolbox[49]. Stimuli were presented on a 17-inch LCD monitor positioned 21 cm from the contralateral eye, spanning 65° (vertical) and 81° (horizontal) of visual space. Stimuli consisted of 100% contrast square wave gratings (spatial frequency 0.04 cycles per degree) drifting in one of eight directions at 2.6 cycles per s. For each trial, one direction was chosen randomly and presented in the following sequence: stationary (1 s), moving (1 s), stationary (1 s).

Virus injections. For injections, long-shanked, volume-calibrated pipettes (Blaubrand) were pulled to achieve a tip size of ~10 µm diameter and tip-filled using negative pressure[50]. Animals were anesthetized as described above, sutures were removed and the Kwik-Sil covering the craniotomy was withdrawn. Injection pipettes were lowered as accurately as possible using the blood vessel pattern and under visual guidance along the same trajectory as recording pipettes to within 100–200 µm of the patched cell. Approximately 150–200 nl of virus solution was injected under 50 mbar of positive pressure for 2–3 min. The pipette was withdrawn, Kwik-Sil re-applied and the animal sutured and allowed to recover.

Tissue processing and imaging. Brains were analyzed 1–9 d after recording. Deeply anaesthetized mice were usually transcardially perfused with cold PBS (0.1 M) followed by 4% paraformaldehyde (wt/wt) in PBS (0.1 M), but sometimes directly decapitated, and the brain was fixed in 4% paraformaldehyde at 4 °C overnight. Coronal brain sections (100–200 µm) were cut on a vibrating microtome (Leica VT1200S or Microm HM 650V) and rinsed in PBS. Fluorescence images were acquired on a Leica SP1, SP5 or a Zeiss 510 laser-scanning confocal microscope. For experiments with biocytin in the intracellular solution, slices were first treated with 1% Triton X-100 (vol/vol) in PBS for 12 h then incubated in a PBS solution containing either Atto-565- or Alexa-488-conjugated streptavidin (Sigma-Aldrich, 1:100–1:200), 5% normal goat serum (vol/vol) and 0.1% Triton X-100 for 12 h at 4 °C. For immunostaining for GFP and mCherry, rabbit anti-GFP (Invitrogen, 1:1,000) and rat anti-RFP primary antibodies (Chromotek, 1:1,000; 24–48 h at 4 °C) were visualized with donkey Alexa-488 anti-rabbit (Invitrogen, 1:500) and goat Alexa-568 anti-rat (Invitrogen, 1:500, 24 h at 4 °C) secondary antibodies. After thorough washing in PBS, slices were mounted with an antifading medium (Mowiol 4-88, Calbiochem + 2.5% DABCO 33-LV, vol/vol, Sigma-Aldrich) and imaged as described above.

48. Kügler, S., Kilic, E. & Bahr, M. Human synapsin 1 gene promoter confers highly neuron-specific long-term transgene expression from an adenoviral vector in the adult rat brain depending on the transduced area. *Gene Ther.* **10**, 337–347 (2003).
49. Brainard, D.H. The psychophysics toolbox. *Spat. Vis.* **10**, 433–436 (1997).
50. Cetin, A., Komai, S., Eliava, M., Seeburg, P.H. & Osten, P. Stereotaxic gene delivery in the rodent brain. *Nat. Protoc.* **1**, 3166–3173 (2006).